# Bandwidth analysis of AC magnetic field sensing based on electronic spin double-resonance of nitrogen-vacancy centers in diamond

AUTHOR(S):

Yamaguchi, Tatsuma; Matsuzaki, Yuichiro; Saito, Shiro; Saijo, Soya; Watanabe, Hideyuki; Mizuochi, Norikazu; Ishi-Hayase, Junko

CITATION:

Yamaguchi, Tatsuma ...[et al]. Bandwidth analysis of AC magnetic field sensing based on electronic spin double-resonance of nitrogen-vacancy centers in diamond. Japanese Journal of Applied Physics 2019, 58(10): 100901.

ISSUE DATE:

2019-09-06

URL:

http://hdl.handle.net/2433/244336

Japanese Journal of Applied Physics

The Japan Society of Applied Physics

**RAPID COMMUNICATION** • **OPEN ACCESS**

# Bandwidth analysis of AC magnetic field sensing based on electronic spin double-resonance of nitrogen-vacancy centers in diamond

Japanese Journal of Applied Physics **58**, 100901 (2019) **RAPID COMMUNICATION**
https://doi.org/**10.7567/1347-4065/ab3d03**

# Bandwidth analysis of AC magnetic field sensing based on electronic spin double-resonance of nitrogen-vacancy centers in diamond

Tatsuma Yamaguchi[1], Yuichiro Matsuzaki[2†], Shiro Saito[2], Soya Saijo[1], Hideyuki Watanabe[3], Norikazu Mizuochi[4], and Junko Ishi-Hayase[1,5*]

[1]*School of Fundamental Science and Technology, Keio University, 3-14-1 Hiyoshi, Kohoku-ku, Yokohama 223-8522, Japan*
[2]*NTT Basic Research Laboratories, NTT Corporation, 3-1 Morinosato-Wakamiya, Atsugi, Kanagawa, 243-0198, Japan*
[3]*Electroinformatics Group, Nanoelectronics Research Institute, National institute of Advanced Industrial Science and Technology (AIST), Central2, 1-1-1 Umezono, Tsukuba, Ibaraki 305-8568, Japan*
[4]*Institute for Chemical Research, Kyoto University, Gokasho, Uji, Kyoto 611-0011, Japan*
[5]*Center for Spintronics Research Network, Keio University, 3-14-1 Hiyoshi, Kohoku-ku, Yokohama 223-8522, Japan*

*E-mail: hayase@appi.keio.ac.jp
†Present address: Electroinformatics Group, Nanoelectronics Research Institute, National institute of Advanced Industrial Science and Technology (AIST), Central2, 1-1-1 Umezono, Tsukuba, Ibaraki 305-8568, Japan

Received July 16, 2019; accepted August 19, 2019; published online September 6, 2019

We have recently demonstrated an AC magnetic field sensing scheme using a simple continuous-wave optically detected magnetic resonance of nitrogen-vacancy centers in diamond. This scheme is based on electronic spin double-resonance excited by continuous microwave and radiofrequency (RF) fields. Here, we measure and analyze the double-resonance spectrum and magnetic field sensitivity for various microwave and RF frequencies. We observe a clear anticrossing of RF-dressed electronic spin states in the spectrum and estimate the bandwidth to be approximately 5 MHz at a center frequency of 9.9 MHz. © 2019 The Japan Society of Applied Physics

A nitrogen-vacancy (NV) center is a defect in diamond where two adjacent carbon atoms are replaced by a nitrogen and a vacancy. It is possible to initialize the electronic spin states of negatively charged NV centers by illuminating them with green laser light.[1)] Additionally, photoluminescence from NV centers provides a way to read out spin states.[2,3)] Moreover, spin states can be manipulated with microwave pulses,[4)] and the coherence time of an NV center can be as long as 2 ms even at room temperature.[5)] These properties show the potential for NV centers to be used in hybrid devices[6–9)] and high-performance magnetic field sensors[10–12)] in a wide range of applications, including, among others, vector magnetic field sensing[13–20)] and magnetic field imaging.[15,21–23)]

In conventional AC magnetic field sensing, pulsed-optically detected magnetic resonance (pulsed-ODMR) has been used.[10,11)] Although pulsed-ODMR provides high sensitivity, it requires sophisticated calibration of the pulse control. In particular, the detection of high-frequency AC magnetic fields using conventional pulsed-ODMR is technically challenging because of the requirement for short pulse intervals (of the order of nanoseconds). Furthermore, AC magnetic field sensing with pulsed-ODMR requires high-speed measurements, and it is not straightforward to obtain these using wide-field imaging with CCD cameras, which do not have a sufficiently rapid response.[15)]

Recently, our group has proposed and demonstrated a novel technique for AC magnetic field sensing with continuous-wave ODMR (CW-ODMR), which does not require pulse control or high-speed measurements. This scheme is based on double-resonance of sublevels of spin-triplet states of NV centers excited by simultaneous application of microwaves and radiofrequency (RF) fields.[24)] The microwaves probe NV centers dressed by the RF fields, which correspond to the target AC magnetic fields. In the ground state manifolds of the NV centers, there are three states, for example, $|B\rangle$, $|D\rangle$, and $|0\rangle$. These states are eigenstates of spin triplets of NV centers under the application of stress or an electric field. When the RF field is resonant with the transition between $|B\rangle$ and $|D\rangle$, there are changes in the ODMR spectrum as the microwave frequency is swept. Such changes in ODMR signals allow detection of AC magnetic fields.

In Ref. 24, AC magnetic field sensing with CW-ODMR was demonstrated with a fixed frequency resonant with the transition between $|B\rangle$ and $|D\rangle$. However, for practical purposes, it is important to determine the bandwidth of an AC magnetic field sensor. In this paper, we investigate the frequency dependence of the sensitivity of an AC magnetic field sensor using CW-ODMR to estimate the bandwidth. We perform a double-resonance experiment with CW-ODMR in which we sweep the frequencies of both the microwave and the RF field. In the spectrum, we clearly observe anticrossing, which corresponds to Autler–Townes (AT) splitting induced by the RF field. We find that the experimental results are consistent with those of theoretical calculations. Finally, we estimate the sensitivity of the AC magnetic field sensor at several frequencies using both experimental and theoretical results, and we again find good agreement between them.

In our experiment, we apply external magnetic fields to obtain a clear spectrum, whereas the previous demonstration of AC magnetic field sensing with CW-ODMR was done without any applied magnetic field.[24)] NV centers have four possible crystallographic axes, and we apply a magnetic field perpendicular to one of these. The magnetic field lifts the degeneracy of the NV centers so that the resonant frequency of one-quarter of the NV centers differs from that of the other NV centers, as shown in Fig. 1. Importantly, with an applied magnetic field of a few millitesla perpendicular to the crystallographic axis, the energy eigenstates are still approximately described by $|0\rangle$, $|B\rangle$, and $|D\rangle$. Thus, AC magnetic fields can induce a transition between $|B\rangle$ and $|D\rangle$, thereby



 

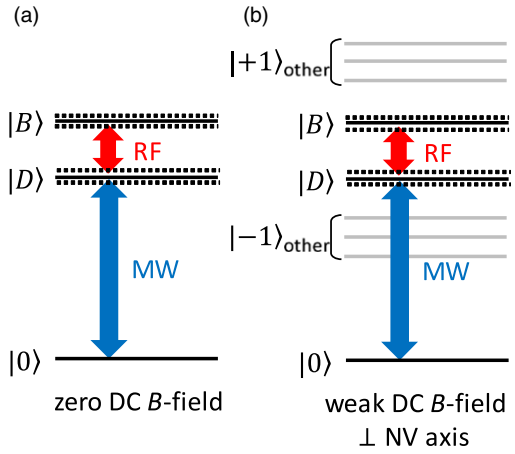


**Fig. 1.** (Color online) Energy levels of NV centers. (a) Without an external DC magnetic field, NV centers with different crystallographic axes have the same resonant frequency, and there are two microwave (MW) resonances in the spectrum. Under resonant excitation by an RF field, there are four MW resonances (dotted lines), which correspond to AT splitting caused by the RF field. (b) With an applied DC magnetic field perpendicular to one of the four possible crystallographic axes, the degeneracy between the axes is lifted, and there are eight MW resonances in the spectrum. By means of frequency selectivity, we focus on the NV centers with axes perpendicular to the applied DC magnetic field.

allowing AC magnetic field sensing with CW-ODMR. We used the orientation being about 40% and liner polarized light, but we applied the lower MW power than Ref. 24, so the contrast in our experiment is around one-quarter of that in Ref. 24. However, we can avoid the mixing of signals from the four different types of NV centers, and so the spectrum becomes much cleaner than that in Ref. 24. This makes it possible for us to perform a systematic study of the bandwidth of the AC magnetic field sensing with CW-ODMR.

For the theoretical part of our results, we apply a magnetic field perpendicular to one of the four possible crystallographic axes. In this setup, we can eliminate the signals from NV centers with the other three crystallographic axes through detuning. Therefore, we perform the theoretical analysis only for those NV centers where the applied magnetic field is perpendicular to the crystallographic axis.The Hamiltonian of the NV center is

$$H_{\mathrm{NV}} = D\hat{S}_z^2 + E_x(\hat{S}_x^2 - \hat{S}_y^2) + E_y(\hat{S}_x\hat{S}_y + \hat{S}_y\hat{S}_x) + g\mu_b B_x\hat{S}_x, \tag{1}$$

where $\hat{S}$ is the spin-1 operator of the electronic spin, $D$ is the zero-field splitting, $E_x$ and $E_y$ are the strains along the $x$ and $y$ directions, and $g\mu_b B_x$ is the Zeeman splitting. In addition, without loss of generality, we can take the magnetic field perpendicular to the crystallographic axis to be in the $x$ direction of the NV center. The ground state is $|0\rangle$, and we define the dark and bright states as $|D\rangle = \frac{1}{\sqrt{2}}(|1\rangle - |-1\rangle)$ and $|B\rangle = \frac{1}{\sqrt{2}}(|1\rangle + |-1\rangle)$, respectively. Under the condition $D \gg g\mu_b B_x^{\prime} \gg E_y$, we can rewrite the Hamiltonian as

$$H \simeq D'\hat{S}_z^2 + E_x'(\hat{S}_x^2 - \hat{S}_y^2), \tag{2}$$

where

$$D' = D + \frac{3}{2}\frac{(g\mu_b B_x)^2}{D + E_x}, \qquad E_x' = E_x + \frac{1}{2}\frac{(g\mu_b B_x)^2}{D + E_x}. \tag{3}$$

This has the same form as the Hamiltonian without an applied magnetic field. Importantly, this analysis shows that the applied magnetic fields increase the effective strain from $E_x$ to $E_x'$. It is known that two dips are observed around 2.87 GHz in CW-ODMR with zero magnetic field. Such dip structures occur when external driving induces transitions from the ground state $|0\rangle$ to another energy eigenstate such as $|B\rangle$ or $|D\rangle$.[25–29] A similar pair of dips should be observed in ODMR in our setup owing to the form of the Hamiltonian in Eq. (2).

Let us consider the dynamics of the NV centers with driving fields. In our experiment, we performed double-resonance spectroscopy by simultaneously applying microwave and RF fields. Here, the RF fields correspond to the target AC magnetic fields. The Hamiltonian of the driving fields is

$$H_{\mathrm{ex}} = \sum_{j=x,y,z} \gamma_e B_{\mathrm{MW}}^{(j)}\hat{S}_j \cos(\omega_{\mathrm{MW}} t) + \gamma_e B_{\mathrm{AC}}^{(j)}\hat{S}_j \cos(\omega_{\mathrm{AC}} t), \tag{4}$$

where $\gamma_e$ is the gyromagnetic ratio of the electron spin, $B_{\mathrm{MW}}$ and $B_{\mathrm{AC}}$ are the amplitudes of the microwave and RF fields respectively, and $\omega_{\mathrm{MW}}$ and $\omega_{\mathrm{AC}}$ are their respective driving frequencies. The total Hamiltonian of an NV center with driving fields is $H = H_{\mathrm{NV}} + H_{\mathrm{ex}}$. In a rotating frame with $U = -\omega_{\mathrm{AC}}|D\rangle\langle D| - \omega_{\mathrm{MW}}|0\rangle\langle 0|$, the effective Hamiltonian is

$$\begin{aligned} H \simeq\ & (D - \omega_{\mathrm{MW}} + E_x)|B\rangle\langle B| \\ & + (D - \omega_{\mathrm{MW}} - E_x + \omega_{\mathrm{AC}})|D\rangle\langle D| \\ & + \tfrac{1}{2}\gamma_e B_{\mathrm{MW}}^{(x)}(|B\rangle\langle 0| + |0\rangle\langle B|) \\ & + \tfrac{1}{2}\gamma_e B_{\mathrm{AC}}^{(z)}(|B\rangle\langle D| + |D\rangle\langle B|), \end{aligned} \tag{5}$$

where we have used the rotating wave approximation. Because we consider an ensemble of NV centers, we can treat the system as a harmonic oscillator, and so the Hamiltonian can be written as

$$H' = \omega_b\hat{b}^\dagger\hat{b} + \omega_d\hat{d}^\dagger\hat{d} + J(\hat{b}^\dagger\hat{d} + \hat{b}\hat{d}^\dagger) + \lambda_b(\hat{b} + \hat{b}^\dagger), \tag{6}$$

where $\omega_b = D + E - \omega_{\mathrm{MW}}$, $\omega_d = D - E - \omega_{\mathrm{MW}} + \omega_{\mathrm{AC}}$, $J = \frac{1}{2}\gamma_e B_{\mathrm{AC}}^{(z)}$, and $\lambda_b = \frac{1}{2}\gamma_e B_{\mathrm{MW}}^{(x)}$. This Hamiltonian shows that the states $|B\rangle$ or $|D\rangle$ are coupled by the applied RF fields (which correspond to the target AC magnetic fields), resulting in RF-dressed states of the NV centers between $|B\rangle$ or $|D\rangle$. From the Heisenberg equation, we obtain

$$\begin{aligned} \frac{d\hat{b}}{dt} &= -i\omega_b\hat{b} - iJ\hat{d} - i\lambda_b - \Gamma_b\hat{b}, \\ \frac{d\hat{d}}{dt} &= -i\omega_d\hat{d} - iJ\hat{b} - \Gamma_d\hat{d}, \end{aligned} \tag{7}$$

where $\Gamma_b$ and $\Gamma_d$ are the decay rates of the states $|B\rangle$ and $|D\rangle$, respectively. Because the system becomes steady in CW-ODMR, we set $d\hat{b}/dt = d\hat{d}/dt = 0$ and obtain

$$\hat{b} = \frac{-\lambda_b(\omega_d - i\Gamma_d)}{(\omega_b - i\Gamma_b)(\omega_d - i\Gamma_d) - J^2},$$
$$\hat{d} = \frac{\lambda_b J}{(\omega_b - i\Gamma_b)(\omega_d - i\Gamma_d) - J^2}. \quad (8)$$

The probability of the state remaining as $|0\rangle$ is $p_0 = 1 - \hat{b}^\dagger\hat{b} - \hat{d}^\dagger\hat{d}$. This probability corresponds to the amount of photoluminescence in the ODMR. From the above expressions, we can calculate the resonant frequency of the microwaves as

$$\omega_{\mathrm{MW}} = \frac{1}{2}\{2D \pm \omega_{\mathrm{AC}} \pm \sqrt{(2E_x - \omega_{\mathrm{AC}})^2 + (\gamma_e B_{\mathrm{AC}}^{(z)})^2}\}, \quad (9)$$

and so there are four resonances in the ODMR, which correspond to AT splitting caused by the RF field on resonant excitation. We can calculate the sensitivity to magnetic fields as

$$\delta B_{\mathrm{AC}}^{(z)} = \frac{\delta S}{|dp_0/dB_{\mathrm{AC}}^{(z)}|}, \quad (10)$$

where $\delta S$ is the standard deviation of the signal.

We now describe our experimental setup to investigate the bandwidth of AC magnetic field sensing with CW-ODMR. We used the same experimental setup in Ref. 24 except applying a DC magnetic field. To apply the DC magnetic field perpendicular to one of the crystallographic axes of the NV centers, we used a magnet positioned under the antenna. To measure the photons emitted from the NV centers, a single-photon-resolving detector was used.

We explain our results as follows. We used the same diamond sample that was used in the experiment in Ref. 24 where we adopt fabrication techniques introduced in Refs. 5,30,31. First, we measured the ODMR without an AC magnetic field, sweeping the microwave frequency as shown in Fig. 2(a). We observe two resonances in this frequency range, as expected from the form of the Hamiltonian in Eq. (2), and these resonances indicate the transitions from $|0\rangle$ to $|B\rangle$ and $|D\rangle$. The difference in contrast for the two peaks observed in Fig. 2(a) comes from the difference in microwave reflection for each frequency. From this result, the frequency difference between $|B\rangle$ and $|D\rangle$ is determined to be 9.9 MHz. This frequency difference is larger than that observed in Ref. 24, which can be explained by the applied orthogonal magnetic fields as described in Eq. (3).

Second, we performed a double-resonance experiment. More specifically, we measured the ODMR by applying both microwave and RF (AC magnetic) fields and sweeping the frequencies of both, as shown in Fig. 2(b). The microwave field causes a transition between $|0\rangle$ and the RF-dressed states, and a reduction in photoluminescence occurs owing to this resonance. Importantly, we observe anticrossing in Fig. 2(b) when the RF frequency is around 9.9 MHz. This corresponds to the transition frequency between $|B\rangle$ and $|D\rangle$ with AT splitting caused by the RF field. By contrast, when the RF frequency is much smaller than 9.9 MHz, the RF fields are well detuned, resulting in reduction of the contrast of the peak in the spectrum. When we use the RF driving with nearly zero frequency, the spectrum is similar to the conventional ODMR which shows two large peaks corresponding to the bright state and dark state of the NV centers. From the ODMR, we determine the resonant frequency by a Lorentzian fitting. In Fig. 2(c), we compare these experimental results with the analytical solution given by Eq. (9), and we find that there is generally a good match between theory and experiment, except for small resonances observed in experiments where the RF frequency is below 4 MHz and the microwave frequency is above 2.890 GHz or below 2.877 GHz. These small resonances might come from a two-photon process that violates the rotating wave approximation. However, such an analysis is complicated and out of the scope of this paper, and so their investigation is left as a topic of future work.

Finally, we measured the bandwidth of AC magnetic field sensing with double-resonance CW-ODMR. The sensitivity depends on the strength of the microwave driving. In the weak driving regime, the signal increases as the microwave driving strength increases, while the linewidth has low dependence on the driving. Meanwhile, in the strong driving regime, the signal intensity does not have a high dependence on the driving strength while the linewidth increases owing to the power broadening as the driving strength increases.

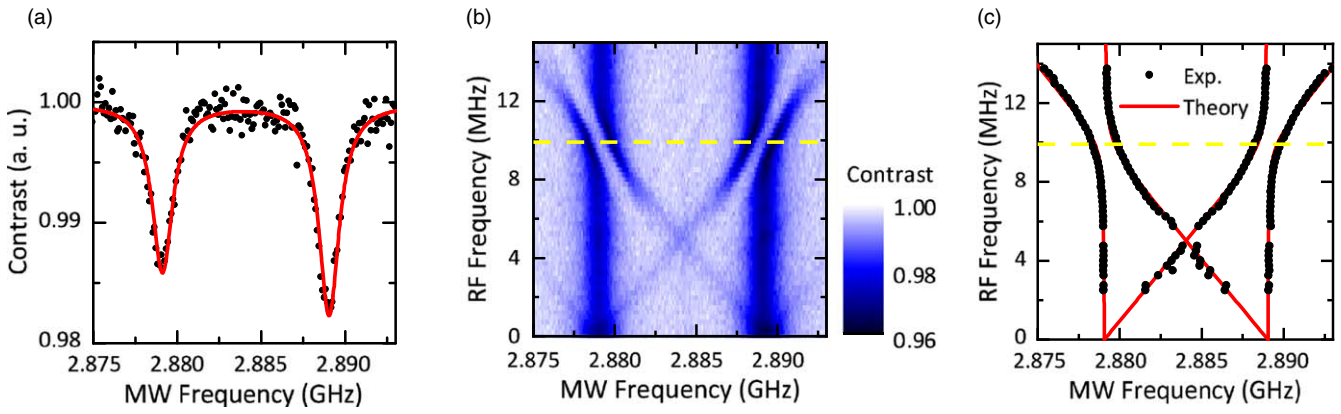


**Fig. 2.** (Color online) (a) CW-ODMR spectrum with applied magnetic field perpendicular to one of the four possible crystallographic axes. We observe resonances corresponding to $|B\rangle$ and $|D\rangle$ of the NV centers with axes perpendicular to the magnetic field, while other NV centers with different axes are detuned by the magnetic field. (b) CW-ODMR with different frequencies of the microwave and AC magnetic (RF) fields. The degree of color shading indicates the amount of photoluminescence. A clear anticrossing structure is observed around $|B\rangle$–$|D\rangle$ resonance (shown by dotted line), and this is a manifestation of the RF-dressed states $|B\rangle$ and $|D\rangle$. (c) Comparison between theory and experiment. The resonant frequency observed in the experiment is plotted, and these data are fitted to the theoretical formula in Eq. (9). There is generally good agreement between theory and experiment.

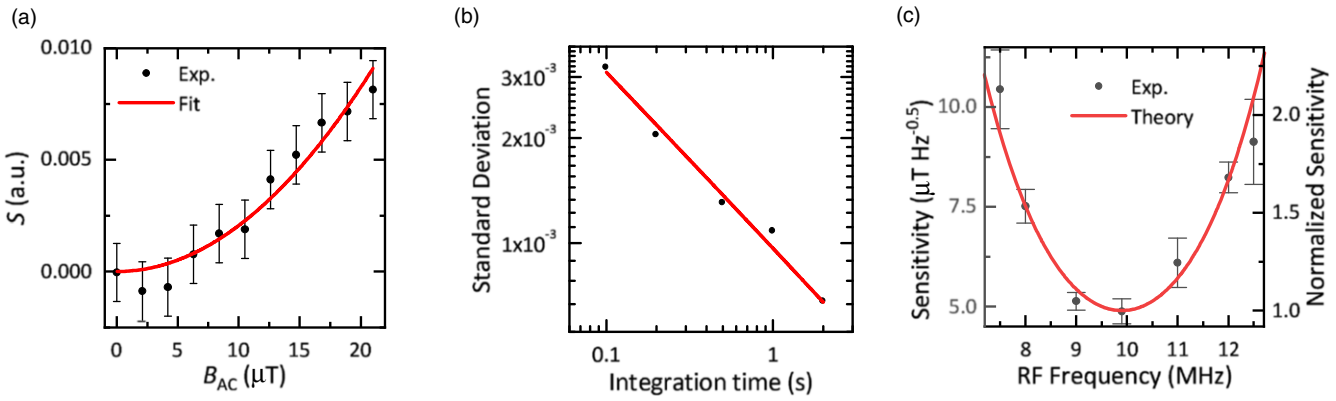


**Fig. 3.** (Color online) (a) Optical signal strength plotted against amplitude of the AC magnetic field (RF) in CW-ODMR. Here, the frequency of the AC magnetic field is fixed at 9.9 GHz. The signal shows a quadratic dependence on the amplitude, and we fit these results using the same method as in Ref. 24. (b) Plot of the standard deviation of the signal in CW-ODMR against time. (c) Plot of the sensitivity of AC magnetic field sensing with CW-ODMR against magnetic field frequency. The bandwidth is estimated to be approximately 5 MHz.

Therefore we choose the microwave driving strength based on when the power broadening starts being observed. Here, the microwave frequency for ODMR was fixed at $\omega_{MW} = D + 0.5\omega_{AC}$ to measure an AC magnetic field with a frequency $\omega_{AC}$. The sensitivity can be estimated from the signal change in ODMR and the signal fluctuations.[24] As contrast (or the inverse of linewidth) increases, the sensitivity linearly increases owing to the larger signal change in the ODMR. We plot the signal change and fluctuations for $\omega_{AC} = 9.9\,\mathrm{MHz}$ in Figs. 3(a), 3(b). In our setup, the sensitivity is around $4.9\,\mu\mathrm{T}/\sqrt{\mathrm{Hz}}$, which is comparable with the sensitivity in the previously demonstrated AC magnetic field sensing with CW-ODMR.[24] Similarly, we estimate the sensitivity at different frequencies of the target AC magnetic fields, and we plot it in Fig. 3(c), where we have normalized the sensitivity using the value at a frequency $\omega_{AC} = 9.9\,\mathrm{MHz}$. We have also fitted these experimental results with our theoretical formula in Eq. (10), using $\Gamma_b = \Gamma_d = \Gamma$ as a fitting parameter. We find good agreement between theory and experiment, obtaining $\Gamma \simeq 2\,\mathrm{MHz}$, which is roughly consistent with the linewidth observed in the ODMR in Fig. 2(a). These results show that the bandwidth of our AC magnetic field sensor is approximately 5 MHz. The bandwidth depends significantly on the linewidth.

In conclusion, we have analyzed the bandwidth of AC magnetic field sensing using CW-ODMR based on electronic spin double-resonance of NV centers in diamond. We have performed CW-ODMR by applying both microwave and RF fields with various frequencies. Consequently, we have observed an anticrossing structure in the spectrum, which agrees with our theoretical prediction. This corresponds to AT splitting of RF-dressed states. Based on these results, we have investigated the sensitivity of AC magnetic field sensing at several frequencies. We find that the bandwidth is approximately 5 MHz at a center frequency of 9.9 MHz. At the center frequency, the sensitivity of our setup is estimated to be $4.9\,\mu\mathrm{T}/\sqrt{\mathrm{Hz}}$. Our results pave the way to the realization of a practical AC magnetic field sensor using a simple CW-ODMR setup. Furthermore, we expect these results to provide the basis for application of the phenomenon involving coupling between $|B\rangle$ and $|D\rangle$. While we are preparing our manuscript, we recognize a similar paper that is also related to the double-resonance spectrum,[32] which may be useful for AC magnetic field sensing with CW-ODMR.

**Acknowledgments** We thank H. Toida and K. Kakuyanagi for helpful discussions. This work was supported by CREST (JPMJCR1774) and by MEXT KAKENHI (Grant Nos. 15H05868, 15H05870, 15H03996, 26220602, and 26249108), and Q-LEAP.

**ORCID iDs** Norikazu Mizuochi https://orcid.org/0000-0003-3099-3210

1) J. Harrison, M. J. Sellars, and N. B. Manson, J. Lumin. **107**, 245 (2004).
2) A. Gruber, A. Dräbenstedt, C. Tietz, L. Fleury, J. Wrachtrup, and C. V. Borczyskowski, Science **276**, 2012 (1997).
3) F. Jelezko, I. Popa, A. Gruber, C. Tietz, J. Wrachtrup, A. Nizovtsev, and S. Kilin, Appl. Phys. Lett. **81**, 2160 (2002).
4) F. Jelezko, T. Gaebel, I. Popa, A. Gruber, and J. Wrachtrup, Phys. Rev. Lett. **92**, 076401 (2004).
5) G. Balasubramanian et al., Nat. Mater. **8**, 383 (2009).
6) X. Zhu et al., Nature **478**, 221 (2011).
7) Y. Kubo et al., Phys. Rev. Lett. **107**, 220501 (2011).
8) Y. Matsuzaki et al., Phys. Rev. Lett. **114**, 120501 (2015).
9) T. Tashima, H. Morishita, and N. Mizuochi, Phys. Rev. A **100**, 023801 (2019).
10) J. M. Taylor, P. Cappellaro, L. Childress, L. Jiang, D. Budker, P. R. Hemmer, A. Yacoby, R. Walsworth, and M. D. Lukin, Nat. Phys. **4**, 810 (2008).
11) T. Wolf, P. Neumann, K. Nakamura, H. Sumiya, T. Ohshima, J. Isoya, and J. Wrachtrup, Phys. Rev. X **5**, 041001 (2015).
12) G. Balasubramanian et al., Nature **455**, 648 (2008).
13) B. J. Maertz, A. P. Wijnheijmer, G. D. Fuchs, M. E. Nowakowski, and D. D. Awschalom, Appl. Phys. Lett. **96**, 092504 (2010).
14) S. Steinert, F. Dolde, P. Neumann, A. Aird, B. Naydenov, G. Balasubramanian, F. Jelezko, and J. Wrachtrup, Rev. Sci. Instrum. **81**, 043705 (2010).
15) L. M. Pham et al., New J. Phys. **13**, 045021 (2011).
16) A. K. Dmitriev and A. K. Vershovskii, J. Opt. Soc. Am. B **33**, B1 (2016).
17) S. Kitazawa, Y. Matsuzaki, S. Saijo, K. Kakuyanagi, S. Saito, and J. Ishi-Hayase, Phys. Rev. A **96**, 042115 (2017).
18) J. M. Schloss, J. F. Barry, M. J. Turner, and R. L. Walsworth, Phys. Rev. Appl. **10**, 034044 (2018).
19) P. Wang, Z. Yuan, P. Huang, X. Rong, M. Wang, X. Xu, C. Duan, C. Ju, F. Shi, and J. Du, Nat. Commun. **6**, 6631 (2015).
20) K. Yahata, Y. Matsuzaki, S. Saito, H. Watanabe, and J. Ishi-Hayase, Appl. Phys. Lett. **114**, 022404 (2019).
21) Y. Hatano, T. Sekiguchi, T. Iwasaki, M. Hatano, and Y. Harada, Phys. Status Solidi A **215**, 1800254 (2018).
22) D. Le Sage, K. Arai, D. R. Glenn, S. J. Devience, L. M. Pham, L. Rahn- Lee, M. D. Lukin, A. Yacoby, A. Komeili, and R. L. Walsworth, Nature **496**, 486 (2013).
23) S. Steinert, F. Ziem, L. T. Hall, A. Zappe, M. Schweikert, N. Götz, A. Aird, G. Balasubramanian, L. Hollenberg, and J. Wrachtrup, Nat. Commun. **4**, 1607 (2013).

24) S. Saijo, Y. Matsuzaki, S. Saito, T. Yamaguchi, I. Hanano, H. Watan-abe, N. Mizuochi, and J. Ishi-Hayase, Appl. Phys. Lett. **113**, 082405 (2018).
25) X. Zhu, Y. Matsuzaki, R. Amsüss, K. Kakuyanagi, T. S. Oka, N. Mizuochi, K. Nemoto, K. Semba, W. J. Munro, and S. Saito, Nat. Commun. **5**, 3524 (2014).
26) L. Rondin, J. P. Tetienne, T. Hingant, J. F. Roch, P. Maletinsky, and V. Jacques, Rep. Prog. Phys. **77**, 056503 (2014).
27) Y. Matsuzaki, H. Morishita, T. Shimooka, T. Tashima, K. Kakuyanagi, K. Semba, W. J. Munro, H. Yamaguchi, N. Mizuochi, and S. Saito, J. Phys.: Condens. Matter **28**, 275302 (2016).
28) T. Mittiga et al., Phys. Rev. Lett. **121**, 246402 (2018).
29) K. Hayashi et al., Phys. Rev. Appl. **10**, 034009 (2018).
30) E. E. Kleinsasser, M. M. Stanfield, J. K. Q. Banks, Z. Zhu, W. D. Li, V. M. Acosta, H. Watanabe, K. M. Itoh, and K. M. C. Fu, Appl. Phys. Lett. **108**, 202401 (2016).
31) H. Watanabe, T. Kitamura, S. Nakashima, and S. Shikata, J. Appl. Phys. **105**, 093529 (2009).
32) A. K. Dmitriev, H. Y. Chen, G. D. Fuchs, and A. K. Vershovskii, Phys. Rev. A **100**, 011801 (2019).